

Spin-Dependent High-Order Topological Insulator and Two Types of Distinct Corner Modes in Monolayer FeSe/GdClO Heterostructure

Qing Wang,^{1,2} Rui Song,^{3,1} and Ning Hao^{1,*}

¹Anhui Key Laboratory of Condensed Matter Physics at Extreme Conditions,
High Magnetic Field Laboratory, HFIPS, Anhui,
Chinese Academy of Sciences Hefei, 230031, China

²Science Island Branch of Graduate School, University of Science and Technology of China, Hefei, Anhui 230026, China

³Science and Technology on Surface Physics and Chemistry Laboratory, Mianyang, Sichuan 621908, China

We propose that a spin-dependent second-order topological insulator can be realized in monolayer FeSe/GdClO heterostructure, in which substrate GdClO helps to stabilize and enhance the antiferromagnetic order in FeSe. The second-order topological insulator is free from spin-orbit coupling and in-plane magnetic field. We also find that there exist two types of distinct corner modes residing in intersections of two ferromagnetic edges and two antiferromagnetic edges, respectively. The underlying physics for ferromagnetic corner mode follows a sublattice-chirality-kink picture. More interestingly, ferromagnetic corner mode shows spin-dependent property, which is also robust against spin-orbit coupling. Unexpectedly, antiferromagnetic corner mode can be taken as a typical emergent and hierarchical phenomenon from an array of ferromagnetic corner modes. Remarkably, antiferromagnetic corner modes violate general kink picture and can be understood as bound states of a one-dimensional Schrodinger equation under a connected potential well. Our findings not only provide a promising second-order topological insulator in electronic materials, but uncover some new properties of corner modes in high-order topological insulator.

In conventional d -dimensional topological insulator, $(d - 1)$ -dimensional bulk-boundary correspondence governs the manifestation of boundary states. Recently, this concept is generalized to $(d - n)$ -dimension with $n \in [2, d]$. The relevant quantum state is called d -dimensional n th-order topological state, *i.e.*, high-order topological state (HOTS)[1–12]. As the simplest HOTS, 2D second order topological insulator (SOTI) is ideal to study various exotic properties of HOTS, and a lot of theoretical models are proposed for 2D SOTI. However, different from field of conventional topological states, where topological dictionary is established and many candidate compounds are collected, the material platforms to realize SOTI are very limited. The current experimentally feasible platforms mainly include photonic, phononic, acoustic and microwave- and electrical-circuit artificial systems[13–19]. For the aspect of electronic materials, some carbon-based compounds such as graphdiyne, γ -graphyne, twisted-bilayer graphene, and bismuth heterostructure are theoretically predicted to host 2D SOTS[20–26], but have not been experimentally realized. Furthermore, spinless or spin-polarized feature of these proposals limits studies of spin-dependent physics of 2D SOTI. Therefore, it remains a urgency to explore experimentally feasible electronic materials hosting 2D SOTI, in particular, the spin-dependent 2D SOTI.

Since superconductivity with ultrahigh transition temperature ($>65\text{K}$) was discovered in monolayer FeSe/SrTiO₃ (FeSe/STO)[27], similar heterostructures such as FeSe/Nb:BaTiO₃/KTaO₃, FeSe/MgO, FeSe/AnataseTiO₂(001), and FeSe/EuTiO₃[28–31] have attracted enormous interests in many research fields. In particular, research of monolayer FeSe/STO was

extended to field of topological physics in 2014[32, 33]. The subsequent theoretical work predicted a long-range Neel antiferromagnetic (AFM) order can spontaneously form in monolayer FeSe/SrTiO₃, and a conventional topological insulator can arise by further taking into account spin-orbit coupling (SOC)[34]. However, whether long-range magnetic orders can arise or not in monolayer FeSe/STO is still an experimental debate[34–41], which reduces feasibility to realize conventional topological insulator based on the Neel AFM in such system.

In this work, we find that a long-range Neel AFM order in monolayer FeSe can be stabilized and enhanced through introducing a ferromagnetic (FM) insulating substrate GdClO. Such strategy can avoid the debate of magnetism in monolayer FeSe. The stability of the heterostructure is verified by self-consistent first-principles calculations. Once Neel AFM order is generated with aid of substrate GdClO, we find that a 2D SOTI naturally emerges, and is free from SOC and in-plane magnetic field. Interestingly, the 2D SOTI hosts two types of distinct corner modes residing in intersections of two FM edge and two AFM edges, respectively. FM corner modes can be intrinsic or extrinsic depending on global or local crystalline symmetry of four edge boundaries is enforced or not. Furthermore, FM corner modes can be understood by a sublattice-chirality-kink picture and show explicitly spin-dependent properties. This enables one to study spin physics of 2D SOTI. Interestingly, AFM corner modes can be taken as emergent corner modes from an array of FM corner modes. This demonstrates an emergent and hierarchical phenomenon of physics in a very simple and explicit manner. Physically, they violate general kink picture and correspond to the bound

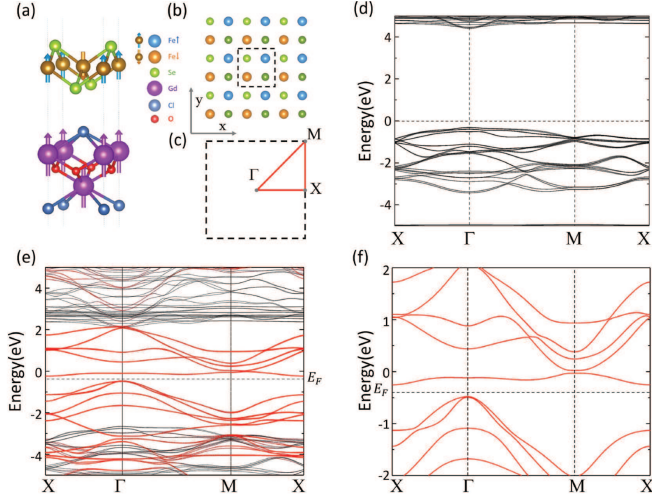


FIG. 1: (a) The spatial configuration of monolayer FeSe/GdClO hetero-structure and the stable magnetic structure from the first-principles calculations. (b) and (c) Lattice structure and Brillouin zone of Neel AFM FeSe. dashed-line square in (b) labels unit cell. (d) The band structure of FM GdClO with slab geometry. (e) The total band structure of monolayer FeSe/GdClO heterostructure with magnetic structure in (a). (f) The bands of free-standing monolayer FeSe by assuming a Neel AFM order. The horizontal dashed lines labeled by E_F in (c) and (d) denote the focused filling level.

states of a one-dimensional Schrodinger equation under a connected potential well.

Inspired by heterostructure of monolayer FeSe/STO, the natural cleavage surface of a promising substrate should be square lattice with matched lattice constant to FeSe. We note that a ready compound GdClO[42–46] fulfills such requirements due to the owned space group $P4/nmm$ symmetry and matched lattice constant as same as FeSe. Fig. 1 (a) shows configuration of FeSe/GdClO heterostructure. It is well-known that GdClO is a FM insulator with a very large gap of 5eV, as shown in Fig. 1 (d). The ferromagnetism is from Gd with magnetic moment $7\mu_B$. Note that Gd atoms have double layer structures, and only the top layer Gd atoms strongly couple to one sublattice of Fe square lattices through van der Waals (vdW) interaction. It is expected that A sublattice of Fe square lattices can arise ferromagnetism with aid of top layer of Gd. However, the magnetism of B sublattice of Fe square lattices cannot be intuitively determined. Thus, we perform the first-principles calculation to consider magnetic configuration of FeSe/GdClO heterostructure. See supplementary materials (SMs) for details. Fig. 1 (a) shows the determined stable magnetic configuration. Interestingly, monolayer FeSe arises a stable long-range Neel AFM order on a FM substrate GdClO. Fig. 1 (e) gives band structures of FeSe/GdClO heterostructure. The electronic states are nearly decoupled between monolayer FeSe and substrate GdClO due

to weak vdW interaction and non charge transfer. Fig. 1 (f) gives band structure of free-standing monolayer FeSe with assumed Neel AFM order. It is as same as FeSe part of FeSe/GdClO heterostructure shown in Fig. 1 (e). Note that some recent works focused on the small gap regime near 0eV at M point in Fig. 1 (f), and discussed possible 2D SOTS induced by SOC and in-plane magnetic field[47, 48]. However, the weakness of SOC and additional magnetic field fine tuning lower the feasibility to realize the 2D SOTS and increase difficulty to study the corner modes protected by the small SOC gap. In the following, we focus on the large gap regime $\sim 0.3\text{eV}$ labeled by E_F in Fig. 1 (e) and (f), and explicitly demonstrate that a pristine 2D SOTS emerges and is free from SOC and in-plane magnetic field.

The bulk topology of such pristine 2D SOTI can be characterized by both a topological invariant and bulk quadrupole moment. From Fig. 1 (b), monolayer Neel AFM FeSe has symmetries of $\hat{P}\hat{T}$, $\{\hat{C}_{2x}|1/2, 0\}$, $\{\hat{C}_{4z}\hat{P}|0, 1/2\}$ and $\{\hat{C}_{4z}\hat{T}|0, 1/2\}$ with \hat{P} , \hat{T} , $\{\hat{E}|1/2, 0\}$ the inversion, time-reversal and fractional translation symmetries, respectively. The topological invariant to characterize bulk topology of 2D SOTI can be calculated with the method developed in a case of chiral HOTS but limited in 2D[4]. Since topological invariant only depends on $\Gamma = (0, 0)$ and $M = (\pi, \pi)$ points, where the representation of fractional translation symmetry $e^{ik_x/y/2}$ takes a value of 1 or i and is redundant. Then, $(\hat{C}_{4z}\hat{P})^4 = -1$, the eigenvalues of $\hat{C}_{4z}\hat{P}$ are four roots of -1 . Due to $[\hat{C}_{4z}\hat{P}, \hat{P}\hat{T}] = 0$ and $\hat{P}\hat{T}$ being anti-unitary, they have to come in complex-conjugated pairs $\{\xi e^{i\pi/4}, \xi e^{-i\pi/4}\}$ with $\xi = 1$ or -1 . The topological invariant can be defined as,

$$(-1)^{v_c} = \prod_{n=1}^{N/2} \xi_{n,\Gamma} \xi_{n,M}. \quad (1)$$

Here, N labels the number of filled bands. The monolayer Neel AFM FeSe has 22 occupied bands, and calculated 11 ξ values at Γ/M points are $\xi_{(1\dots 11),\Gamma/M} = (\pm 1, -1, \pm 1, \mp 1, \mp 1, 1, -1, 1, \mp 1, \mp 1, \pm 1)$. This yields $v_c = 1$ explicitly confirming a 2D SOTI. In the pioneer work of HOTS[1, 2], the high-order topology can also be understood from change of bulk charge dipole moment $p_{x/y}$ and quadrupole moment q_{xy} , which are defined as

$$p_{x/y} = \frac{e}{2} \left(\sum_n 2p_{x/y}^n \bmod 2 \right), \quad (2)$$

$$q_{xy} = \frac{e}{2} \left(\sum_n 2p_x^n p_y^n \bmod 2 \right). \quad (3)$$

Here, $p_{x/y}^n = q_{x/y}^n/2$ with $q_{x/y}^n$ fulfilling the equation $(-1)^{q_{x/y}^n} = \eta^n(M)/\eta^n(\Gamma)$. $\eta^n(M/\Gamma)$ denotes the n th band's eigenvalue of $\hat{C}_{4z}\hat{P}$ at M/Γ point with $\eta =$

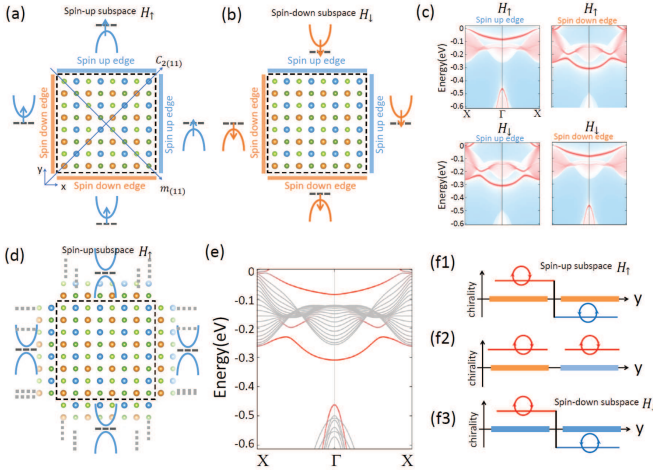


FIG. 2: (a)-(b) Illustration of monolayer Neel AFM FeSe cluster with size of 4×4 in unit of unit cells shown in Fig. 1 (b). (c) The edge spectrum of spin-up and -down Hamiltonian H_{\uparrow} and H_{\downarrow} , respectively. The relevant spin-polarized half massive Dirac bands are schematically plotted near four edges of cluster in (a) and (b). (d) The full massive Dirac bands can be obtained by sticking two parallel edges corresponding to (a). (e) The full edge spectrum without spin-resolved property. (f1)-(f3) Three kinds of sublattice chirality kinks for three types of corners in (a) and (b).

$\xi e^{\pm i\pi/4}$. Note that $p_x = p_y$ due to $\hat{C}_{4z}\hat{P}$ symmetry, and the summation is over all the occupied bands. The 22 (11 pairs) eigenvalues of $\hat{C}_{4z}\hat{P}$ symmetry at M/Γ point are listed in SMs. Then, $(p_x, p_y) = 0$ and $q_{xy} = e/2$, respectively. This supports a 2D SOTI in monolayer Neel AFM FeSe/GdClO.

From the generalized bulk-boundary correspondence, a 2D SOTI enables existence of 0d corner modes. Fig. 2 (a) shows a typical cluster of monolayer Neel AFM FeSe. It has two kinds of corners formed by two edges with the same and opposite FM orders, respectively. The existence of corner modes can be understood under following sublattice-chirality-kink picture. From edge spectrum in Fig. 2 (c) and (e), two spatially separated one dimensional massive Dirac bands at two parallel x or y edges can be recombined by sticking two parallel edges together in each spin polarization subspace, as shown in Fig. 2 (a) and (d). Then, a low-energy effective Hamiltonian to describe the edge spectrum can be expressed as

$$H_{\uparrow, x/y}(k_{x/y}) = \pm v k_{x/y} \tau_{y/x} + m \tau_z, \quad (4)$$

$$H_{\downarrow, x/y}(k_{x/y}) = \pm v k_{x/y} \tau_{y/x} - m \tau_z, \quad (5)$$

Here, v is an effective velocity. $k_{x/y}$ are momenta along x/y direction, $\tau_{x/y/z}$ are three Pauli matrices defined in sublattice space with intertwined orbital degree of freedom. m is the mass induced by the AFM order. The

cluster in Fig. 2 (a) has $\hat{P}\hat{T}$, $\hat{C}_{2(1,1)}\hat{T}$ and $\hat{m}_{(1,1)}$ symmetries, and two different corners formed by intersections of two same and opposite FM edges, respectively. Note that $\hat{C}_{2(1,1)}\hat{T}$ builds intra-spin-subspace connection, and $\hat{P}\hat{T}$ and $\hat{m}_{(1,1)}$ constructs inter-spin-subspace connection. Consider orbital weight of bulk bands near E_F in Fig. 1 (e), the basis functions of Hamiltonian in Eqs. (4) and (5) can be defined as $\psi_{\uparrow}(k) = [d_{A,z^2,\uparrow}(k), d_{B,xz+iyz,\uparrow}(k)]^T$ [32, 33] and $\psi_{\downarrow} = \hat{P}\hat{T}\psi_{\uparrow}(k)$ (See Fig. S1 in SMs). Then, the representation matrix U of $\hat{C}_{2(1,1)}\hat{T}$ is $\frac{1}{2}[(1+\tau_z) - i(1-\tau_z)]\mathcal{K}$ with \mathcal{K} the complex conjugate. For instance, in spin-up subspace, $UH_{\uparrow,x}(k_x)U^{\dagger}|_{k_x \rightarrow -k_y} = vk_y\tau_x + m\tau_z$. In comparison with $H_{\uparrow,y}(k_y)$, the sublattice chirality defined by $\vec{k} \times \vec{\tau}$ changes sign. Namely, there exists a sublattice-chirality kink, as shown in Fig. 2 (f1). Thus, a corner mode must appear for the corner formed by two same FM edges [49]. However, for the corner formed by two opposite FM edges, $H_{\uparrow,x}(k_x) \xrightarrow{\hat{m}_{(1,1)}} H_{\downarrow,y}(k_y) \xrightarrow{\hat{P}\hat{T}} H_{\uparrow,y}(k_y)$. Namely, two edge Hamiltonian are identical under $\hat{m}_{(1,1)}$ in the restricted $H_{\uparrow}(k)$ subspace, as shown in Fig. 2 (f2). Thus, no zero mode will emerge. Similarly, in spin-down subspace, another corner mode appears from the sublattice-chirality-kink picture, as shown in Fig. 2 (f3). Fig. 3 (a) gives the spectrum of the cluster. One can find two degenerate corner modes located on two corners from two same FM edges. Clusters with other patterns and the relevant spectrum are shown in SMs. Note that corner modes are robust against SOC and in-plane magnetic field (See Fig. S3 and S4 in SMs). Different from robustness of topological boundary states in conventional topological insulator, the corner modes in 2D SOTI depend on details of patterns of the clusters (See Fig. S2 in SMs). Thus, the role of crystalline symmetry is subtle. The 2D SOTI can be intrinsic if four edges is globally considered and $\hat{C}_{2(1,1)}\hat{T}$ is enforced. Otherwise, the 2D SOTI can be extrinsic if two edges are considered locally [6, 50, 51]. In any case, two FM edges connected by $\hat{C}_{2(1,1)}\hat{T}$ is the key to enable appearance of corner mode.

Different from previous proposals, above spin-dependent sublattice-chirality-kink picture indicates the FM corner modes should also be spin-dependent. Fig. 3 (b) and (c) give the spin-dependent spectrum and distribution of the spin-polarized corner modes. The location of corner modes can be understood from Fig. 3 (d) and (e), where the strong and weak hopping integrals are schematically plotted in spin-up and -down subspace, respectively (See Fig. S6 in SMs). The strong bonds of iron atoms at left-lower and top right corners are broken in spin-up and -down subspace, respectively. This leaves the relevant corners with isolated spin-dependent corner modes in Fig. 3 (b)-(e). Note that the fidelity of spin polarization is 99.6% with SOC, because spin-dependent nature is governed by magnetic splitting with energy scale 2.5eV in comparison to tiny SOC energy

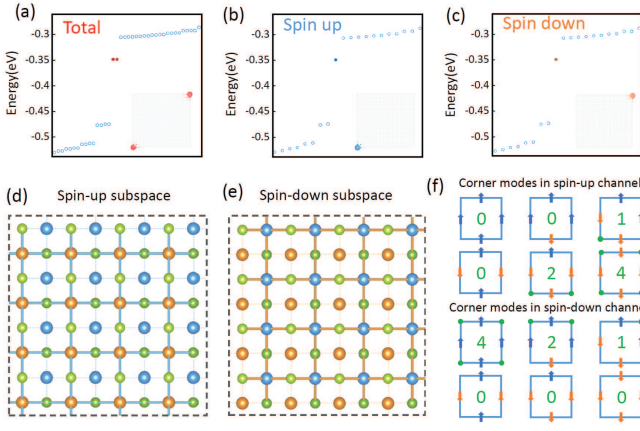


FIG. 3: (a)-(c) The discrete energy spectrum of cluster in Fig. 2 (a) without SOC. (a) for no spin-resolved case and (b), (c) for spin-dependent cases. The inserts in (a)-(c) give the density distribution of the corner modes. The cluster size takes 20×20 in calculations. (d) and (e) The relative hopping integral patterns between Fe $xz/yz/z^2$ and Se z orbital for two spin-decoupled Hamiltonian without SOC, respectively. The strong and weak hoppings are labeled by thick and thin connections, respectively. (f) The summary of distribution of corner modes with definite spin-up and -down polarization in several different of clusters, respectively.

$\sim 0.03\text{eV}$. It indicates spin-dependent feature is robust against other weak external perturbations and enables ones to manipulate spin degree of freedom of corner modes in possible application. In Fig. 3 (f), we list various possibilities to realize corner modes in two spin channels.

The cluster of FeSe/GdClO can have distinct AFM edges as shown in Fig. 4 (a). Fig. 4 (b) and (c) give the relevant edge spectrum. The remarkable feature is emergence of two nearly flat bands near $E_F \sim -0.35\text{eV}$. Their formation can be understood according to Fig. 4 (d), in which the strong and weak hopping integrals are labeled in spin-up and -down subspace, respectively. Then, each spin-down and -up iron atom with broken strong bonds can bound a corner mode, as shown in top and bottom panels in Fig. 4 (d), respectively. The isolated corner modes arrange to one-dimensional array and has weak coupling to form two degenerate flat bands shown in Fig. 4 (b). SOC can further induce weak coupling to break the degeneracy of flat bands shown in Fig. 4 (c). Numerical calculations for square cluster with four AFM edges indicate there exist four different AFM corner modes with each four quadruple degeneracies, as shown in Fig. 4 (f). The AFM corner modes have lower energy than bottom of flat bands. It indicates the general kink picture is violated. Interestingly, we find that AFM corner modes can be understood by following one-dimensional Schrodinger equation through considering the edge mapping shown in

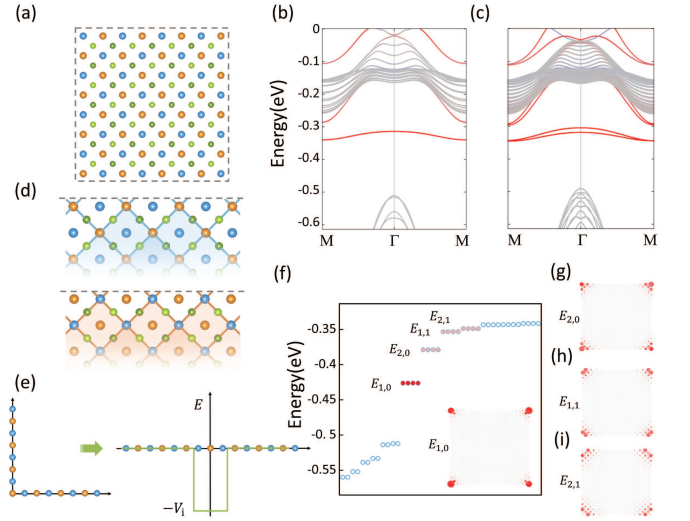


FIG. 4: (a) A cluster of monolayer FeSe with size 4×4 in unit of $\sqrt{2}$ unit cell shown in Fig. 1 (b). The cluster size is 14×14 in calculation of (e)-(h). (b)-(c) The AFM edge spectrum without SOC and with SOC, respectively. (d) The relative hopping integral patterns for decoupled spin-up (top panel) and -down (bottom panel) Hamiltonian without SOC, respectively. (e) The mapping of two AFM edges from orthogonal to linear configuration. (f) The discrete energy spectrum corresponds to (a). The insert gives the density distribution of the corner mode with four-quadruple degeneracy and the lowest energy. (f)-(h) The density distribution of other three corner modes with increasing energy.

Fig. 4 (e),

$$H_{AFM}(k \rightarrow -i\partial_x)\psi(x) = E\psi(x), \quad (6)$$

with

$$H_{AFM}(k \rightarrow -i\partial_x) = -\frac{\hbar^2}{2m^*} \frac{d^2}{dx^2} + V(x). \quad (7)$$

Here, m^* is effective mass of flat bands. $V(x)$ is effective potential well near a corner of two AFM edges. $V(x)$ can be approximately expressed by a square potential well. $V(x) = -V_i$ when $|x| < a/2$ and otherwise $V(x) = 0$. Here, a denotes width of the potential. i is 1 or 2 to label two different flat bands. The bound-state solutions of Eq. (6) are standard. The even-parity solution is $E_{i,n} = \frac{\pi^2 \hbar^2}{2m^* a^2} (2n+1)^2 - V_i$ and $\psi_n(x) \sim \cos k_n x$ for $|x| < a/2$ and $\sim e^{-\alpha_n |x|}$ for $|x| > a/2$. The odd-parity solution is $E_{i,n} = \frac{\pi^2 \hbar^2}{2m^* a^2} (2n+2)^2 - V_i$ and $\psi_n(x) \sim \sin k_n x$ for $|x| < a/2$ and $\sim e^{-\alpha_n |x|}$ for $|x| > a/2$. n takes 0, 1, 2... The numerical results in Fig. 4 (f) indicate the emergent four different corner modes correspond to $E_{1,0}$, $E_{2,0}$, $E_{1,1}$, $E_{2,1}$ with consistent even and odd alternating distribution patterns as shown in Fig. 4 (f)-(i). It seems that the AFM corner modes are not topologically protected. However, their emergence can be stretched back

to FM corner modes. Thus, both FM and AFM corner modes are topologically protected in a different hierarchical manner. Note that there exists at least a AFM corner mode for any $V(x)$ well.

In many previous proposals, in-plane external magnetic field or magnetic proximity effect is induced to drive 2D SOTI. The corner modes are sensitive to these fine tunings. It improves difficulties to construct electronic devices based on corner modes. The 2D SOTI and relevant corner modes here are robust against in-plane external magnetic field, and other perturbations (See Fig. S3-S5 in SMs). The corner modes here lie at 0.35eV below original Fermi energy. To experimentally detect them, scanning tunnelling spectroscopy is a feasible technique, which can measure spin-resolved local density of states by changing voltage in a large regime. The transport properties of the corner modes can be studied only when their energy is tuned to the Fermi level. Such tuning can be experimentally realized by electrostatic gating or proton gating techniques, both of which are mature and have especial advantages in layered heterostructures[52–54]. In particular, such gated tuning has been realized in FeSe thin flakes[55–57]. Once appropriate hole carriers are induced by gating to move corner mode energy to Fermi energy, monolayer FeSe/GdClO could be an ideal platform to study the properties of 2D SOTI and relevant corner modes.

In conclusion, we propose that a monolayer FeSe/GdClO heterostructure can realize a 2D second-order topological insulator, which is free from SOC and in-plane magnetic field, Furthermore, we find that corner modes are protected by a large gap of about 0.3eV, and can be detected at high temperature. We also find there exist two distinct types of FM and AFM corner modes. More interestingly, we show that FM corner modes follow a sublattice-chirality-kink picture and have unique spin-dependent property, and AFM corner modes emerge from FM corner mode array. The diversity of FM and AFM corner modes provide new way to construct the relevant devices by utilizing their spin degree of freedom.

We thank Lin Hao for helpful discussions. This work was financially supported by National Natural Science Foundation of China under Grants (No. 12022413, No. 11674331), the National Key R&D Program of China (Grant No. 2017YFA0303201), the “Strategic Priority Research Program (B)” of the Chinese Academy of Sciences, Grant No. XDB33030100, the Collaborative Innovation Program of Hefei Science Center, CAS (Grants No. 2020HSC-CIP002), the Major Basic Program of Natural Science Foundation of Shandong Province (Grant No. ZR2021ZD01). A portion of this work was supported by the High Magnetic Field Laboratory of Anhui Province, China.

* Electronic address: haon@hmfl.ac.cn

- [1] W. A. Benalcazar, B. A. Bernevig, and T. L. Hughes, Electric multipole moments, topological multipole moment pumping, and chiral hinge states in crystalline insulators, *Phys. Rev. B* **96**, 245115 (2017).
- [2] W. A. Benalcazar, B. A. Bernevig, and T. L. Hughes, Quantized electric multipole insulators, *Science* **357**, 61-66 (2017).
- [3] Z. Song, Z. Fang, and C. Fang, (d-2)-dimensional edge states of rotation symmetry protected topological states, *Phys. Rev. Lett.* **119**, 246402 (2017).
- [4] F. Schindler, A. M. Cook, M. G. Vergniory, Z. Wang, S. S. P. Parkin, B. A. Bernevig, and T. Neupert, Higher-order topological insulators, *Science Advances* **4**, 10.1126/sciadv.aat0346 (2018).
- [5] G. van Miert and C. Ortix, Higher-order topological insulators protected by inversion and rotoinversion symmetries, *Phys. Rev. B* **98**, 081110 (2018).
- [6] E. Khalaf, Higher-order topological insulators and superconductors protected by inversion symmetry, *Phys. Rev. B* **97**, 205136 (2018).
- [7] M. Geier, L. Trifunovic, M. Hoskam, and P. W. Brouwer, Second-order topological insulators and superconductors with an order-two crystalline symmetry, *Phys. Rev. B* **97**, 205135 (2018).
- [8] D. Călugăru, V. Juričić, and B. Roy, Higher-order topological phases: A general principle of construction, *Phys. Rev. B* **99**, 041301 (2019).
- [9] Y. Ren, Z. Qiao, and Q. Niu, Engineering corner states from two-dimensional topological insulators, *Phys. Rev. Lett.* **124**, 166804 (2020).
- [10] C.-A. Li and S.-S. Wu, Topological states in generalized electric quadrupole insulators, *Phys. Rev. B* **101**, 195309 (2020).
- [11] Y.-B. Yang, K. Li, L.-M. Duan, and Y. Xu, Type-ii quadrupole topological insulators, *Phys. Rev. Research* **2**, 033029 (2020).
- [12] M. Jung, Y. Yu, and G. Shvets, Exact higher-order bulk-boundary correspondence of corner-localized states, *Phys. Rev. B* **104**, 195437 (2021).
- [13] S. Mittal, V. V. Orre, G. Zhu, M. A. Gorlach, A. Poddubny, and M. Hafezi, Photonic quadrupole topological phases, *Nature Photonics* **13**, 692 (2019).
- [14] L. He, Z. Addison, E. J. Mele, and B. Zhen, Quadrupole topological photonic crystals, *Nature Communications* **11**, 3119 (2020).
- [15] M. Serra-Garcia, V. Peri, R. Susstrunk, O. R. Bilal, T. Larsen, L. G. Villanueva, and S. D. Huber, Observation of a phononic quadrupole topological insulator, *Nature* **555**, 342 (2018).
- [16] Y. Qi, C. Qiu, M. Xiao, H. He, M. Ke, and Z. Liu, Acoustic realization of quadrupole topological insulators, *Phys. Rev. Lett.* **124**, 206601 (2020).
- [17] C. W. Peterson, W. A. Benalcazar, T. L. Hughes, and G. Bahl, A quantized microwave quadrupole insulator with topologically protected corner states, *Nature* **555**, 346 (2018).
- [18] S. Imhof, C. Berger, F. Bayer, J. Brehm, L. W. Molenkamp, T. Kiessling, F. Schindler, C. H. Lee, M. Greiter, T. Neupert, and R. Thomale, Topoelectrical-circuit realization of topological corner modes, *Nature*

- Physics **14**, 925 (2018).
- [19] M. Serra-Garcia, R. Sussstrunk, and S. D. Huber, Observation of quadrupole transitions and edge mode topology in an lc circuit network, *Phys. Rev. B* **99**, 020304 (2019).
- [20] E. Lee, R. Kim and J. Ahn et al. Two-dimensional higher-order topology in monolayer graphdiyne. *npj Quantum Materials* **5**, 1-7 (2020).
- [21] X. Sheng, C. Chen and H. Liu et al. Two-dimensional second-order topological insulator in graphdiyne. *Phys. Rev. Lett.* **123**, 256402 (2019).
- [22] B. Liu, G. Zhao and Z. Liu et al. Two-dimensional quadrupole topological insulator in γ -graphyne. *Nano. Lett.* **19**, 6492-6497 (2019).
- [23] M. Park, Y. Kim and G. Cho et al. Higher-order topological insulator in twisted bilayer graphene. *Phys. Rev. Lett.* **123**, 216803 (2019).
- [24] C. Ma, Q. Wang and S. Mills et al. Moiré band topology in twisted bilayer graphene. *Nano. Lett.* **20**, 6076-6083 (2020).
- [25] B. Liu, L. Xian and H. Mu et al. Higher-order band topology in twisted moiré superlattice. *Phys. Rev. Lett.* **126**, 066401 (2021).
- [26] C. Chen, Z. Song, J. Zhao, Z. Chen, Z. Yu, X. Sheng and S. A. Yang Universal Approach to Magnetic Second-Order Topological Insulator, *Phys. Rev. Lett.* **125**, 056402 (2020).
- [27] Q. Y. Wang, Z. Li, W. H. Zhang, Z. C. Zhang, J. S. Zhang, W. Li, H. Ding, Y. B. Ou, P. Deng, K. Chang et al., Interface Induced High Temperature Superconductivity in Single Unit-Cell FeSe Films on SrTiO₃, *Chin. Phys. Lett.* **29**, 037402 (2012).
- [28] R. Peng, H. C. Xu, S. Y. Tan, H. Y. Cao, M. Xia, X. P. Shen, Z. C. Huang, C.H.P. Wen, Q. Song, T. Zhang, B. P. Xie, X. G. Gong and D. L. Feng, Tuning the band structure and superconductivity in single-layer FeSe by interface engineering, *Nat. Commun.* **5**, 5044 (2014).
- [29] J. Shiogai, Y. Ito, T. Mitsuhashi, T. Nojima and A. Tsukazaki, Electric-field-induced superconductivity in electrochemically etched ultrathin FeSe films on SrTiO₃ and MgO, *Nat. Phys.* **12**, 42–46 (2016).
- [30] H. Ding, Y. Lv, K. Zhao, W. Wang, L. Wang, C. Song, X. Chen, X. Ma, and Q. Xue, High-Temperature Superconductivity in Single-Unit-Cell FeSe Films on Anatase TiO₂(001), *Phys. Rev. Lett.* **117**, 067001 (2016).
- [31] C. Liu, H. Shin, A. Doll, H. Kung, Ryan P. Day, B. A. Davidson, J. Dreiser, G. Levy, A. Damascelli, C. Piamonteze, and K. Zou, High-temperature superconductivity and its robustness against magnetic polarization in monolayer FeSe on EuTiO₃, *npj Quantum Mater.* **6** 85 (2021).
- [32] N. Hao and J. Hu, Topological Phases in the Single-Layer FeSe, *Phys. Rev. X* **4**, 031053 (2014).
- [33] N. Hao and J. Hu, Topological quantum states of matter in iron-based superconductors: from concept to material realization, *Natl. Sci. Rev.* **6**, 213-226 (2019).
- [34] Z. F. Wang,, H. Zhang, D. Liu, C. Liu, C. Tang, C. Song, Y. Zhong, J. Peng, F. Li, C. Nie, L. Wang, X. Zhou, X. Ma., Q. Xue and F. Liu, *Nat. Mater.* **15**, 968 (2016).
- [35] F. Zheng, Z. Wang, W. Kang and P. Zhang, Antiferromagnetic FeSe monolayer on SrTiO₃: The charge doping and electric field effects, *Sci Rep* **3**, 2213 (2013).
- [36] K. Liu, Z. Lu, and T. Xiang, Atomic and electronic structures of FeSe monolayer and bilayer thin films on SrTiO₃ (001): First-principles study, *Phys. Rev. B* **85**, 235123 (2012)
- [37] H. Cao, S. Chen, H. Xiang, and X. Gong, Antiferromagnetic ground state with pair-checkerboard order in FeSe, *Phys. Rev. B* **91**, 020504(R) (2015).
- [38] S. Y. Tan, et al. Interface-induced superconductivity and strain-dependent spin density wave in FeSe/SrTiO₃ thin films. *Nat. Mater.* **12**, 634–640 (2013).
- [39] H. Y. Cao, S. Y. Tan, H. J. Xiang, D. L. Feng, and X. G. Gong, Interfacial effects on the spin density wave in FeSe/SrTiO₃ thin films. *Phys. Rev. B* **89**, 014501 (2014).
- [40] Y. Zhou, L. Miao, P. Wang, F. F. Zhu, W. X. Jiang, S. W. Jiang, Y. Zhang, B. Lei, X. H. Chen, H. F. Ding, Hao Zheng, W. T. Zhang, Jin-feng Jia, Dong Qian, and D. Wu, Antiferromagnetic Order in Epitaxial FeSe Films on SrTiO₃, *Phys. Rev. Lett.* **120**, 097001 (2018).
- [41] Y. Gu, Q. Wang, H. Wo, Z. He, H. C. Walker, J. T. Park, M. Enderle, A. D. Christianson, W. Wang, J. Zhao, Frustrated magnetic interactions in FeSe, *arXiv:2207.10981* (2022).
- [42] C. Bungenstock, T. Tröster, W. B. Holzapfel, L. Fini and M. Santoro, Energy levels of Pr³⁺:GdOCl under pressure, *J. Phys.: Condens. Matter* **12** 6959, (2000).
- [43] K. R. Kort and S. Banerjee, Oriented Electrophoretic Deposition of GdOCl Nanoplatelets, *J. Phys. Chem. B* **117**, 1585-1591 (2013).
- [44] C. Bungenstock, T. Tröster, W. B. Holzapfel, Effect of pressure on free-ion and crystal-field parameters of Pr³⁺ in LOCl (L=La, Pr, Gd), *Phys. Rev. B* **62**, 7945 (2000).
- [45] M. R. Osanloo1, M. L. Van de Put, A. Saadat and W. G. Vandenberghe, Identification of two-dimensional layered dielectrics from first principles, *Nat. Commun.* **12**, 5051 (2021).
- [46] D. Boglajenkova, A. Andersenb, S. M. Healdc, T. Vargab, D. R. Mortensend, S. Tetefer, G. T. Seidlere, N. Govindf, T. G. Levitskaiaa, X-ray absorption spectroscopy of trivalent Eu, Gd, Tb, and Dy chlorides and oxchlorides, *Journal of Alloys and Compounds*, **897**, 162629 (2022).
- [47] Aiyun Luo, Zhida Song and Gang Xu, Fragile topological band in the checkerboard antiferromagnetic monolayer FeSe, *npj Comput. Mater.* **8**, 26 (2022)
- [48] Haimen Mu, Gan Zhao, Huimin Zhang and Zhengfei Wang, Antiferromagnetic second-order topological insulator with fractional mass-kink, *npj Comput. Mater.* **8**, 82 (2022).
- [49] R. Jackiw and C. Rebbi, Solitons with fermion number 1/2, *Phys. Rev. D* **13**, 3398 (1976).
- [50] E. Khalaf, W. A. Benalcazar, T. L. Hughes, and R. Queiroz, Boundary-obstructed topological phases, *Phys. Rev. Research* **3**, 013239 (2021).
- [51] L. Trifunovic and P. W. Brouwer, Higher-Order Topological Band Structures, *Phys. Status Solidi B* **258**, 2000090 (2021).
- [52] J. T. Ye, S. Inoue, K. Kobayashi, Y. Kasahara, H. T. Yuan, H. Shimotani and Y. Iwasa, Liquid-gated interface superconductivity on an atomically flat film, *Nat. Mater.* **9**, 125–128 (2009).
- [53] J. T. Ye , Y. J. Zhang, R. Akashi, M. S. Bahramy, R. Arita, and Y. Iwasa, Superconducting dome in a gate-tuned band insulator, *Science* **338**, 1193–1196 (2012).
- [54] D. Costanzo, S. Jo, H. Berger and A. F. Morpurgo, Gate-induced superconductivity in atomically thin MoS₂ crystals, *Nat. Nanotechnol.* **11**, 339–344 (2016).
- [55] B. Lei, J. H. Cui, Z. J. Xiang, C. Shang, N. Z. Wang,

- G. J. Ye, X. G. Luo, T. Wu, Z. Sun, and X. H. Chen, Evolution of high-temperature superconductivity from a low- T_c phase tuned by carrier concentration in FeSe thin flakes. *Phys. Rev. Lett.* **116**, 077002 (2016).
- [56] B. Lei, N. Z. Wang, C. Shang, F. B. Meng, L. K. Ma, X. G. Luo, T. Wu, Z. Sun, Y. Wang, Z. Jiang, B. H. Mao, Z. Liu, Y. J. Yu, Y. B. Zhang, and X. H. Chen, Tuning phase transitions in FeSe thin flakes by field-effect transistor with solid ion conductor as the gate dielectric. *Phys. Rev. B* **95**, 020503 (2017).
- [57] C. S. Zhu, J. H. Cui, B. Lei, N. Z. Wang, C. Shang, F. B. Meng, L. K. Ma, X. G. Luo, T. Wu, Z. Sun, and X. H. Chen, Tuning electronic properties of $\text{FeSe}_{0.5}\text{Te}_{0.5}$ thin flakes using a solid ion conductor field-effect transistor. *Phys. Rev. B* **95**, 174513 (2017).